Aalborg Universitet

A modification on velocity terms of Reynolds equation in a spherical coordinate system

Renani, Ehsan Askari; Andersen, Michael Skipper

A modification on velocity terms of Reynolds equation in a spherical coordinate system

E. Askari[*1] and M.S. Andersen[1]

[1] Department of Materials and Production, Aalborg University, Aalborg 9220, Denmark

Abstract

The widely-used Reynolds equation to simulate fluid lubrication in hip implants by Goenka and Booker has velocity terms accounting just for the rotational motion of the femoral head. The present study, therefore, hypothesizes that modifying velocity terms being used in Reynolds equation, which capture both translation and rotation of the femoral head, can affect resultant fluid pressure, fluid-film thickness and friction force. To assess such hypothesis, a computational model of a hip implant based on multibody dynamics methodology and Reynold equation is developed. It is illustrated that modifying velocities can cause friction forces to increase, significantly, compared to Goenker and Booker's. Moreover, the minimum film thickness and maximum fluid pressure undergo notable decreases during the swing and stance phases, respectively.

Keywords: Multibody d*ynamics; Reynolds equation; hydrodynamic lubrication; Total hip replacement*

1. Introduction

Friction opposes relative motion of bearing surfaces of a hip implant, sliding against each other. It leads to energy loss and bearing surfaces undergo material loss due to wear occurrence, which can eventually lead to failure of hip implants [1-2]. A remedy to facilitate such relative motion and prevent surfaces to damage is to add lubricant to the joint. As the synovial capsule is preserved in total hip replacement, hip arthroplasty works under lubrication condition [3]. The fluid-film lubrication is built due to the convergence of a film in both space and time, which are associated with so-called wedge-film action and squeeze-film action, respectively [4-6]. Such film actions are function of the velocities of bearing surfaces and bearing geometries.

---

[*] Corresponding author.
E-mail address: ehsanaskary@gmail.com (E. Askari)

Nomenclature

Symbol	Definition	Symbol	Definition
c	Clearance size	Q_1 and Q_2	The points on the head and cup surfaces, respectively
D	Non-dimensional hydrodynamic parameter	R_c	The radius of the cup
$\mathbf{e} = (e_x, e_y, e_z)$	The eccentricity vector in Cartesian coordinate system	t	Time (s)
$e = \|\mathbf{e}\|$	The size of eccentricity vector	U_θ and U_φ	The tangential velocity components at Q_1
$\dot{e}$	The time rate of the size of the eccentricity vector	$\mathbf{V}_{O_b}$	The velocity vector of the head center
$\mathbf{e}_{r_e}, \mathbf{e}_{\theta_e}$ and $\mathbf{e}_{\varphi_e}$	The local orthogonal unit vectors at the head center	$\mathbf{V}_{Q_1}$	The velocity vector at point Q_1
$\mathbf{e}_r, \mathbf{e}_\theta, \mathbf{e}_\varphi$	The local orthogonal unit vectors	$\mathbf{V}_{Q_1}^n$	Normal velocity vector at the point Q_1
$\mathbf{F}$	The force vector	$\mathbf{V}_{Q_1}^t = \left(V_{Q_1,x}^t, V_{Q_1,y}^t, V_{Q_1,z}^t\right)$	Tangential velocity vector at the point Q_1
$\mathbf{f} = (f_x, f_y, f_z)$	Physiological force vector and its components	$\mathbf{V}_{Q_1/O_b}$	The velocity vector of point Q_1 with respect to the head center
$\mathbf{f}^\mu = (f_x^\mu, f_y^\mu, f_z^\mu)$	Friction force vector	y_n	The state variable of the system at time t_n
$\mathbf{f}^L = (f_x^L, f_y^L, f_z^L)$	Resultant fluid force vector		
h	Fluid-film thickness	β	The cup angle
$h_{\min}$	Minimum film thickness	θ and φ	Azimuthal and polar angles
$\mathbf{M}$	The mass matrix of the system	θ_e and φ_e	Azimuthal and polar angles of the eccentricity vector
O_b and O_c	Centers of the femoral head and cup, respectively	$\Delta\theta$ and $\Delta\varphi$	Element size in azimuthal and polar directions
P	Fluid pressure	$\mathbf{\Omega} = (\omega_x, \omega_y, \omega_z)$	Angular velocity vector
$_i^n P, i = 1\ldots6$	The pressure profile at time t_n and the ith increment calculation in the Cash-Karp method	μ	Lubricant viscosity
$\ddot{\mathbf{q}}$	The acceleration vector	τ_θ and τ_φ	Shear stresses
q	The size of time step	$\mathbf{\nabla}$	Del (nabla) in the spherical coordinate system

Analysis of lubricated hip implants was pioneered by Goenka and Booker in 1980 [7], where a finite element model to explore hydrodynamic lubrication was developed, followed by Ai and Chen (1996) while solving Reynolds equation using the finite difference method [7-8]. A couple of years later, Jin and Dowson (1999) performed a hydrodynamic analysis of hip arthroplasties under three-dimensional loadings and motion, taking both entraining and squeeze film into account [9]. Jin and his colleagues made use of a general film thickness equation already developed by Hamrock and Dowson to evaluate the factors influencing film thickness, e.g. clearance size. Hamrock and Dowson equation accounts for the pressure-dependent property of the lubricant and elastic deformation of joint components, obtained for the fluid lubrication of a ball on a plane [10]. In the next decade, the study of elastohydrodynamic lubrication in hip prostheses became very demanding as it was found out that elastic deformation of hip components contribute

to fluid-film lubrication significantly. Jin and his colleagues, Jagatia and Jalali-Vahid, published two papers on this topic while one of them concentrated on just entraining motion and another squeeze-film motion [11-12]. The elastic deformation of hip components was treated by means of the column method for polyethylene cup and the displacement coefficients matrix acquired using finite element method. Elastohydrodynamic lubrication of hip prostheses for different materials, loading and motion, transient and steady-state modes, Newtonian and non-Newtonian lubricant were studied in details so far [13-20]. However, these studies neglected dynamics and determined magnitude and location of minimum film thickness using a static equilibrium relation between forces generated due to fluid pressure and physiological loadings. Fluid flow in artificial hip joints is formulated using Reynolds equation presented by Goenka and Booker [7], in a spherical coordinate system. They also provided the velocity terms of the journal in both radial and azimuthal directions. However, those velocities do not account for the translational motion of the femoral head, but just rotational motion. According to the definition of velocities of corresponding points, each fixed to one of bearing surfaces, [21], such velocities result from rigid body motion, including both translational and rotational motions of joint components. Moreover, it is well-known that the femoral head freely moves inside the cup, resulting in six-degrees of freedom (DOF) that corresponds to 3D translations and rotations. Regarding Reynolds equation, one can argue that small variations in the velocities could significantly contribute to fluid pressure and minimum film thickness, as important tribological parameters.

Therefore, the present study hypothesizes that modifying the velocity terms used in Reynolds equation, which address both translation and rotation of the femoral head, can affect fluid pressure, fluid-film thickness and friction force. To do so, the Reynolds equation reported by Goenka and Booker are modified such that 3D velocities of the femoral head, representing both rotational and translational motions are included. A multibody dynamics model is constructed, accounting for the dynamics of the femoral head subjected to the normal walking condition and fluid flow is formulated using Reynolds equation. The acetabular cup is assumed stationary while the femoral head is free to move. Both hip components are considered rigid and the squeeze-film action is neglected for the sake of brevity and simplicity. The finite difference method is utilized to discretize the governing equation of lubricant and the Gauss-Seidel relaxation scheme is used to solve discretized equations while the multi-grid method reduces computational time. Fluid-structure interaction between the femoral head and fluid lubrication is taken into account making use of a partitioned method. Finally, results obtained by Reynolds equation reported by Goenka and Booker are compared to those acquired by the modified one by the present study.

2. Mathematical modeling

A malfunctioned natural joint is replaced by a hip prosthesis to relieve pain and restore hip joint function to carry imposed loaded and provide normal human mobility. As the synovial capsule is preserved in total hip

replacement, the hip implant works under lubrication condition [3]. Moreover, such an artificial human joint is a clearance joint due to a difference between the radii of its bearing components [22]. Hence, this is a mechanical system with six degrees of freedom (DOF). The mathematical formulation of hip joint motion, therefore, is to take care of the femoral head motion as well as fluid-film lubrication generated due to rotational and translational relative motion under three-dimensional physiological loadings measured in vivo. Relative rotational movement drags fluid into the fluid-film domain resulting in fluid forces that separate the contacting bodies.

2.1. Multi-body dynamics formulation

In this section, a dynamic model of a hip implant based on the multibody dynamics methodology is set up. The acetabular cup is assumed to be stationary while the femoral head can freely move inside the cup domain [23]. There are no constraints imposed to the system, but the femoral head motion is controlled by the geometry of the articulating bodies, fluid pressure and actuators, e.g. physiological forces and motion. The mass of the femoral head is incorporated into the model [24]. According to in vivo physiological loadings and motion reported by Bergmann et al., three-dimensional loadings are applied at the center of the head and the angular motions of the femoral head are assigned to be those reported in vivo [25-26]. Therefore, degrees of freedom of the system is reduced to three, which correspond to the translational motion of the femoral head. The governing equations of motion are written using Newton's second law for multibody rigid dynamics given by [27-28]

$$\mathbf{M\ddot{q}} = \mathbf{F} \tag{1}$$

in which $\mathbf{M}$ is the mass matrix of the system. $\mathbf{\ddot{q}}$ represents the acceleration vector while the term on the right side denotes the force vector applied on the system. In order to compute the movement of the system, one therefore needs to determine the force vector, $\mathbf{F}$. The forces consist of physiological loadings and those due to gravitational acceleration and fluid-film lubrication, which are considered in the next section.

2.2. Computational fluid dynamics and Modified velocity terms

The Navier-Stokes equations consist of three equations of motion, containing four unknowns, namely pressure and three velocity components. One more equation, enabling us to determine unknowns, is the equation of continuity provided by the principle of mass conservation. The classical Reynolds theory of fluid lubrication simplified the Navier-Stokes equations based on physical observations of fluid lubrication flow.

The lubricant film is assumed to be very thin with negligible curvature and the fluid inertia and body forces were neglected [4, 21].
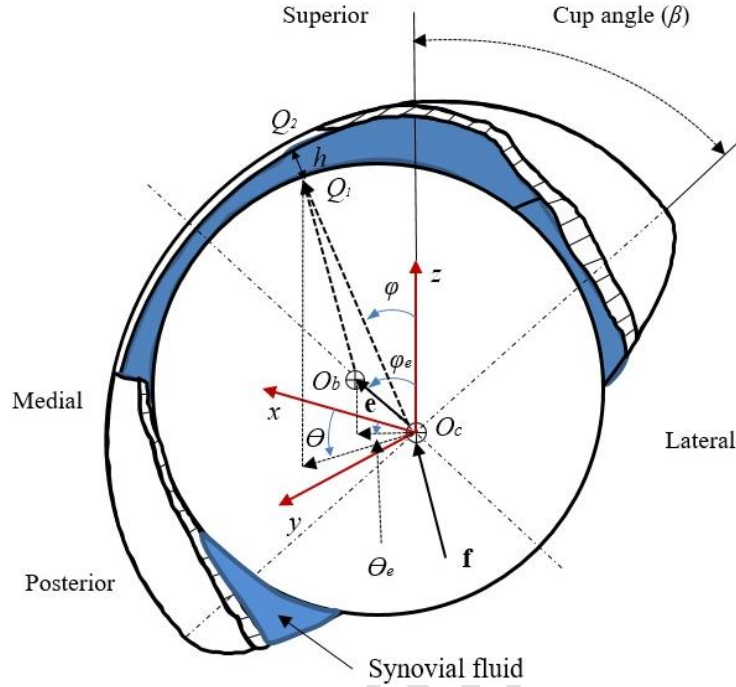

Fig. 1. A schematic representation of a lubricated hip implant

Implementing the aforementioned simplifications to Navier-Stokes equations, the resultant Reynolds equation in a spherical coordinate system can be written as follows, [7]

$$\boldsymbol{\nabla} \cdot \left(\frac{h^3}{12\mu} \boldsymbol{\nabla} P \right) = \boldsymbol{\nabla} \cdot (h\overline{\mathbf{U}}) + \frac{\partial h}{\partial t} \tag{2}$$

where h is the fluid-film thickness at each point of the fluid domain (see Fig.1), which is identified by Θ, φ, i.e. the azimuthal and polar angles of the spherical coordinate system, and c, i.e. clearance size. Fluid pressure is denoted by P while $\overline{\mathbf{U}}$ represents the tangential velocity vector at point Q_1, which belongs to the ball surface, assuming the velocity of point Q_2 locating on the cup surface is zero. The first term on the right-hand side of Eq. (2) is the mathematical representation of wedge-film action while the second term, so-called squeeze-film action, is the relative velocity by which two bodies approach each other in the perpendicular direction. In the present study, the squeeze-film action is neglected to only study the effect of velocity terms of hydrodynamic lubrication. By substituting the velocity vector into the above equation, assuming a constant fluid viscosity, μ, and doing some mathematical manipulation, the Reynolds equation for a spherical joint, like the artificial hip joint, is written by [7]

$$\frac{1}{R_c^2}\left[\frac{1}{\sin\theta}\frac{\partial}{\partial\varphi}\left(\frac{h^3}{12\mu}\frac{\partial P}{\partial\varphi}\right)+\frac{1}{\sin\theta^2}\frac{\partial}{\partial\theta}\left(\frac{h^3}{12\mu}\sin\theta\frac{\partial P}{\partial\theta}\right)\right] \tag{3}$$
$$=\frac{1}{2R_c\sin\theta}\left[h\cos\theta\, U_\theta+h\sin\theta\frac{\partial U_\theta}{\partial\theta}+h\frac{\partial U_\varphi}{\partial\varphi}+U_\theta\sin\theta\frac{\partial h}{\partial\theta}+U_\varphi\frac{\partial h}{\partial\varphi}\right]$$

Goenka and Booker, [7], reported velocity terms, U_θ and U_φ, as follows:

$$U_\theta=-R_c\omega^x\sin\varphi+R_c\omega^y\cos\varphi \tag{4}$$

$$U_\varphi=-R_c\omega^x\cos\varphi\cos\theta-R_c\omega^y\sin\varphi\cos\theta+R_c\omega^z\sin\theta \tag{5}$$

However, in these velocities, the translational motion of the femoral head is neglected.
Taking both rotation and translation in account, tangential velocity $\mathbf{V}_{Q1}^t$ in the Cartesian coordinate system is derived in the present study so that the velocity terms in Eq. (3) in radial and azimuthal directions can be given by

$$U_\theta=\mathbf{V}_{Q1}^t\cdot\mathbf{e}_\theta,\quad U_\varphi=\mathbf{V}_{Q1}^t\cdot\mathbf{e}_\varphi \tag{6}$$

where $\mathbf{V}_{Q1}^t$ represents the tangential velocity at any point, Q_1, illustrated in Fig. 2. As the femoral head can freely move, the velocity of point Q_1 consists of two terms, namely translation and rotation. The velocity is written with respect to the center of cup, as given by (Fig. 2)

$$\mathbf{V}_{Q_1}=\mathbf{V}_{O_b}+\mathbf{V}_{Q_1/O_b} \tag{7}$$

where $\mathbf{V}_{O_b}$ stands for the velocity of the center of ball (femoral head) with respect to the cup center, which is

$$\mathbf{V}_{O_b}=\frac{d}{dt}(\mathbf{e})=\dot{e}\mathbf{e}_{r_e}+e\left(\dot{\theta}_e\mathbf{e}_{\theta_e}+\dot{\varphi}_e\sin\theta_e\mathbf{e}_{\varphi_e}\right) \tag{8}$$

$\mathbf{e}$ depicts the eccentricity vector owing to the translation of the femoral head, as illustrated in Fig. 2, and the subscript 'e' refers to the direction of the eccentricity vector. The rotational motion of the point Q_1 with respect to the local coordinate system attached to the center of the head is written by

$$\mathbf{V}_{Q_1/O_b} = \mathbf{\Omega} \times \overrightarrow{O_bQ_1} \tag{9}$$

in which $\mathbf{\Omega} = (\omega_x, \omega_y, \omega_z)$ is the angular velocity vector and the positon vector of the point Q_1 in the local coordinate system can be given by

$$\overrightarrow{O_bQ_1} = \overrightarrow{O_cQ_1} - \mathbf{e} \tag{10}$$

while its position vector in the reference coordinate system attached to the cup center, $\overrightarrow{O_cQ_1}$, is as follows:

$$\overrightarrow{O_cQ_1} = (R_c - h)\mathbf{e}_r \tag{11}$$

in which $\mathbf{e}_r$ is the unit vector pointing from the origin of the reference coordinate system to the point Q_1 and R_c is the cup radius. According to the eccentricity vector and Eq. (11), Eq. (10) can be recast as

$$\overrightarrow{O_bQ_1} = (R_c - h) \times \left(\sin\theta\cos\varphi\,\hat{\imath} + \sin\theta\sin\varphi\,\hat{\jmath} + \cos\theta\,\hat{k}\right) - \|\mathbf{e}\| \times (\sin\theta_e\cos\varphi_e\,\hat{\imath} \tag{12}$$
$$+ \sin\theta_e\sin\varphi_e\,\hat{\jmath} + \cos\theta_e\,\hat{k})$$

The normal and tangential components of the velocity, respectively, at the point Q_1 can, therefore, be given by (see Fig. 2)

$$\mathbf{V}_{Q1}^n = (\mathbf{V}_{Q1} \cdot \mathbf{e}_r)\mathbf{e}_r \tag{13}$$

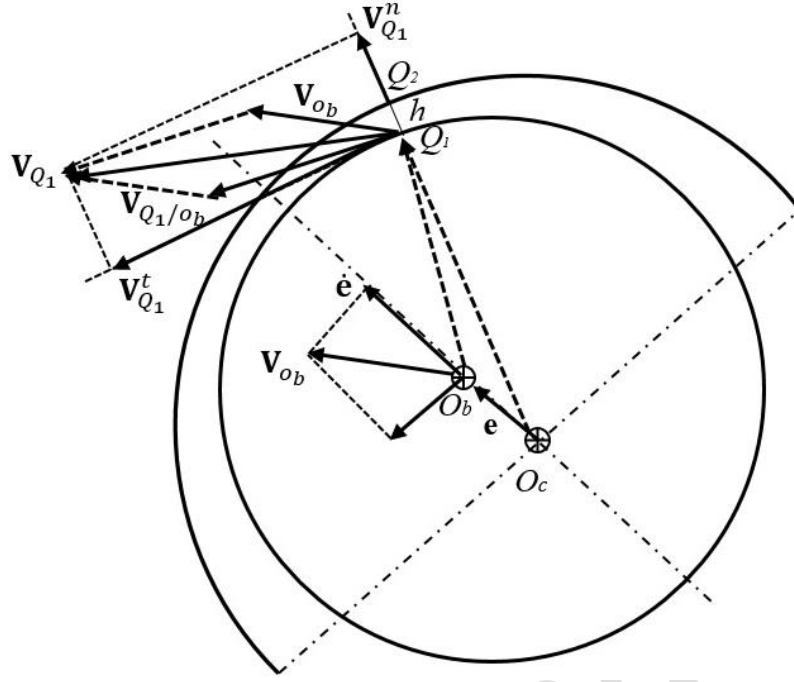$$\mathbf{V}_{Q1}^t = \mathbf{V}_{Q1} - \mathbf{V}_{Q1}^n \tag{14}$$

Fig. 2. A 2-D representation of the contribution of rotational and translational motions in the tangential velocity, $\mathbf{V}_{Q1}^t$, at point Q_1

Now that the modified version of velocities are determined, let's return to Eq. (3) to discuss the solution of Reynolds equation. The first-term on the right side of the equation (3) is the mathematical representative of wedge-film action. Regarding the geometry of hip articulation, fluid-film thickness, h, can be written as a function of clearance size c, eccentricity vector $\mathbf{e} = (e_x, e_y, e_z)$, and the location of point Q_2 specified by Θ and φ as follows

$$h(\varphi, \theta) = c - e_x \sin\theta\cos\varphi - e_y \sin\theta\sin\varphi - e_z \cos\theta \qquad (15)$$

In order to solve numerically the fluid-flow equation, the surface of the acetabulum cup is discretized into $n \times m$ elements with the size $\Delta\theta \times \Delta\varphi$ while the thickness of each element is $h(\varphi, \theta)$ at any time step (t_i). The finite-difference method is employed to discretize Eq. (3), [29]. In order to solve the discrete Reynolds equation, the pressure along the edge of the cup is set to be atmospheric pressure. Moreover, the Swift-Stieber boundary condition is applied to satisfy the cavitation boundary, i.e. $\frac{\partial P}{\partial \theta} = \frac{\partial P}{\partial \varphi} = 0$ and the cavitation pressure is set to be the atmospheric pressure, [21]. It is worth noting that the atmospheric pressure is assumed zero as it does not affect the solution, but facilitate satisfying boundary conditions. The resultant discretized equations are solved using the Gauss-Seidel relaxation method along with the multi-grid method,

[30-31]. The resultant forces due to fluid pressure that are imposed to the femoral head are computed by performing the following integrations over the fluid-film domain.

$$f_x^L = R_c^2 \iint P(\sin\theta)^2 \cos\varphi \, d\theta d\varphi$$

$$f_y^L = R_c^2 \iint P(\sin\theta)^2 \sin\varphi \, d\theta d\varphi \qquad (16)$$

$$f_z^L = R_c^2 \iint P\sin\theta\cos\theta \, d\theta d\varphi$$

2.3. Friction force due to fluid shear stresses

Friction forces due to the fluid shear stresses are generated and imposed to the moving body. These forces contribute to the dynamics and tribology of bearing surfaces. Shear stresses are given as follows [14]

$$\tau_\theta = \frac{\mu}{R_c}\frac{\partial u_\theta}{\partial\theta} = \mu\frac{U_\theta}{h} + \frac{h}{2R_c}\frac{\partial P}{\partial\theta} \qquad (17)$$

$$\tau_\varphi = \frac{\mu}{R_c\sin\theta}\frac{\partial u_\varphi}{\partial\varphi} = \mu\frac{U_\varphi}{h} + \frac{h}{2R_c\sin\theta}\frac{\partial P}{\partial\varphi} \qquad (18)$$

The resulting friction forces are computed by performing an integration of shear stresses over the bearing surfaces as given by

$$f_x^\mu = -R_c^2 \iint \left[\tau_\theta\sin\theta\cos\theta\cos\varphi - \tau_\varphi\sin\varphi\sin\theta\right] d\theta d\varphi$$

$$f_y^\mu = -R_c^2 \iint \left[\tau_\theta\sin\theta\cos\theta\sin\varphi + \tau_\varphi\cos\varphi\sin\theta\right] d\theta d\varphi \qquad (19)$$

$$f_z^\mu = -R_c^2 \iint -\tau_\theta\sin\theta\sin\theta \, d\theta d\varphi$$

while integrands of above integrations are given as functions of tangential velocity, pressure variation and fluid-film thickness at each point, e.g. point Q_1 illustrated in Fig. 1, of the domain of interest, as follows:

$$\tau_\theta\sin\theta\cos\theta\cos\varphi - \tau_\varphi\sin\varphi\sin\theta = \mu\frac{V_{Q_1,x}^t}{h}\sin\theta + \frac{h}{2R_c}\frac{\partial P}{\partial\theta}\sin\theta\cos\theta\cos\varphi - \frac{h}{2R_c\sin\theta}\frac{\partial P}{\partial\varphi}\sin\varphi\sin\theta \qquad (20)$$

$$\tau_\theta \sin\theta\cos\theta\sin\varphi + \tau_\varphi\cos\varphi\sin\theta = \mu\frac{V_{Q_1,y}^t}{h}\sin\theta + \frac{h}{2R_c}\frac{\partial P}{\partial\theta}\sin\theta\cos\theta\sin\varphi + \frac{h}{2R_c\sin\theta}\frac{\partial P}{\partial\varphi}\cos\varphi\sin\theta \tag{21}$$

$$-\tau_\theta\sin\theta\sin\theta d\theta = \mu\frac{V_{Q_1,z}^t}{h}\sin\theta - \frac{h}{2R_c}\frac{\partial P}{\partial\theta}\sin\theta\sin\theta \tag{22}$$

Therefore, the external force applied to the femoral head due to both fluid lubrication and 3-D physiological loadings can be calculated summing the force components presented by Eqs. (16) and (19) as well as the physiological force vector, **f**, reported in Fig. 3, that can be written in a vector form as

$$\mathbf{F} = \mathbf{f} + \mathbf{f}^\mu + \mathbf{f}^L + m\mathbf{g} \tag{23}$$

2.4. Fluid-structure interaction and the solution procedure

Regarding the description of solving the Reynolds equation, Eq. (3), and boundary conditions applied to the fluid domain (see the last paragraph of the section 2.2.), the non-dimensional format of the discrete Reynolds equation is finally written in the following matrix format:

$$C_1 P_{i-1,j} + C_2 P_{i,j} + C_3 P_{i+1,j} + C_4 P_{i,j-1} + C_5 P_{i,j+1} = C_6 \tag{24}$$

where the coefficient matrices can be found in previous works [9]. A Gauss-Seidel relaxation scheme is used along with the multi-grid method, i.e. a three-level V cycle represented in Fig. 3. The Gauss-Seidel method computes the updated pressure at each node, $P_{i,j}^{n+1}$, at time t_{n+1} using pressure magnitudes of surrounding nodes at previous time step, t_n, and next time step, t_{n+1}, as can be seen from Eq. (25).

$$C_2 P_{i,j}^{n+1} = C_6 - C_1 P_{i-1,j}^{n+1} - C_3 P_{i+1,j}^n - C_4 P_{i,j-1}^{n+1} - C_5 P_{i,j+1}^n \tag{25}$$
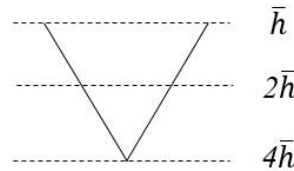

Fig. 3. Three-level V cycle multi-grid method

Interaction between the synovial fluid and the femoral head is also dealt with and explained as follows. The dynamics of the hip articulation as a function of time is a result of interacting bearing structures and

fluid lubricant, which is a multi-physics phenomenon. The present study develops a partitioned approach to take into account the interaction between fluid and structure (FSI). Therefore, the previously developed algorithms of solving each of both fluid and structure as two separate domains are used while they communicate each other by transferring data through their moving interface. The method to solve the equations of motion is a modified adaptive Runge-Kutta-Fehlberg method, i.e. RK45, which is the so-called Cash-Karp method. The partitioned method developed in the present study is embedded into the Cash-Karp method. A schematic representation of the method is depicted in Fig. 4. Using the state space representation, the second order equations of motion, Eq. (1), can be rewritten as a first order equations set as

$$\frac{d\mathbf{y}}{dt} = \mathbf{H}(t, y) \tag{26}$$

where $\mathbf{y}$ is the state variable of the coupled system, which is given by $\mathbf{y} = (\mathbf{q}, \dot{\mathbf{q}})$ in which $\mathbf{q}$ stands for the position vector of the femoral head in the Cartesian coordinate system attached to the center of the cup and $\dot{\mathbf{q}}$ its translational velocity vector. Therefore, $\mathbf{y}$ and $\mathbf{H}$ can be written as follows

$$\mathbf{y} = [q_1, q_2, q_3, \dot{q}_1, \dot{q}_2, \dot{q}_3] \tag{27}$$

$$\mathbf{H} = \left[\dot{q}_1, \dot{q}_2, \dot{q}_3, \frac{F_x}{m}, \frac{F_y}{m}, \frac{F_z}{m}\right] \tag{28}$$

in which $\mathbf{F} = [F_x, F_y, F_z]$ that is calculated at each time step according to Eq. (23) and m presents the mass of the femoral head. Moreover, the implementation of the partitioned procedure is presented in the adaptive Runge-Kutta-Fehlberg method, Eq. (29), in which $\mathbf{y}_n$ is the state variable of the system at the time t_n while $\mathbf{y}_{n+1}$ represents the state variable of the system at next time step. At the previous time step i, the pressure profile is ${}_1^n P$. Regarding the Runge-Kutta-Fehlberg method, after updating the external time-dependent force and rotational motion, the first increment, $\mathbf{k}_1$, based on the slope at the initial point of the time interval is calculated with the pressure profile ${}_1^n P$. The updated pressure is computed as to be ${}_2^n P$, as observed in Fig. 4-2. The second increment is obtained at the time $t_n + c_2 \Delta t$, where Δt represents the size of time step, updated state variables $y_n + \Delta t(a_{21}\mathbf{k}_1)$ and the pressure profile ${}_2^n P$. This procedure continues until all increments according to the Runge-Kutta orders 4 and 5 are determined. The state variables of the system at time t_{n+1} is computed for both corresponding orders, 4 and 5. An error is determined by comparing the state variables obtained from each order of the Runge-Kutta method. Moreover, a threshold error, i.e. 0.1 μ, is defined to which the previous error is compared. If the error magnitude of the adaptive Runge-Kutta method is greater than the threshold error, the time step is halved and the computation is redone. This process continues until the solution converges. It is worth noting that the size of time step, Δt, for the dynamic analysis is 1 μs.

$$\mathbf{y}_{n+1} = \mathbf{y}_n + q \sum_{i=1}^{s} b_i \mathbf{k}_i$$

$$\mathbf{k}_1 = \mathbf{H}(t_n, \mathbf{y}_n) \; with \; P = {}_1^n P$$

$$\mathbf{k}_2 = \mathbf{H}(t_n + c_2 \Delta t, \mathbf{y}_n + \Delta t(a_{21} \mathbf{k}_1)) \; with \; P = {}_2^n P \qquad (29)$$

$$\vdots$$

$$\mathbf{k}_i = \mathbf{H}\left(t_n + c_i \Delta t, y_n + \Delta t(\sum_{j=1}^{i-1} a_{ij} \mathbf{k}_j) \right) \; with \; P = {}_i^n P$$
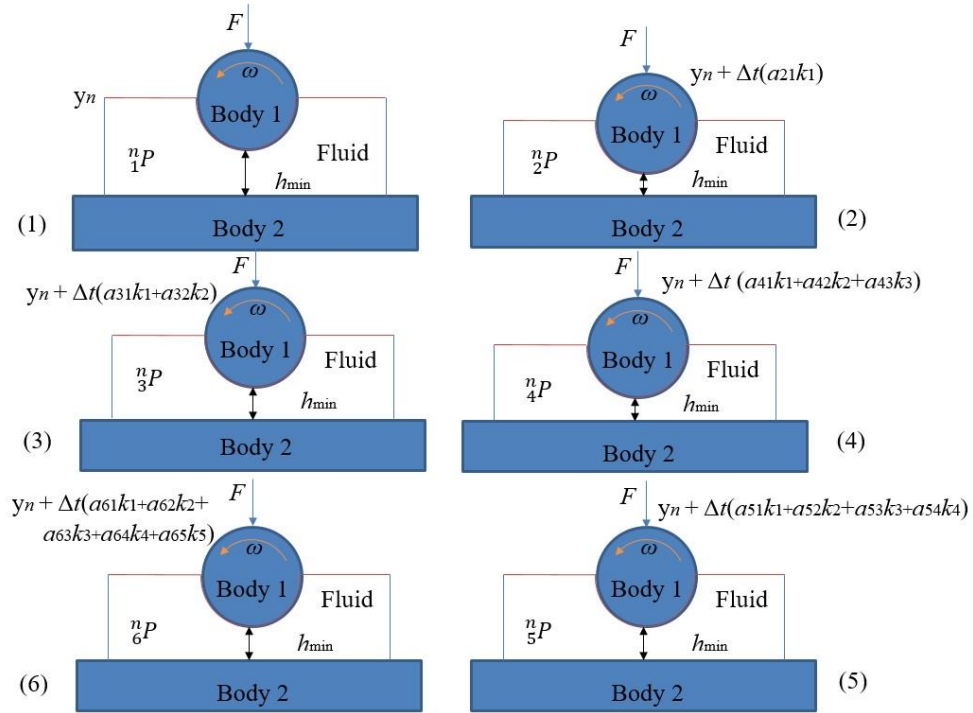

Fig. 4. A schematic representation of a partitioned approach developed for fluid-structure interaction

2.5. A demonstrative example and model validation

The dynamic model developed in the previous section is used to study hydrodynamic lubrication in hip arthroplasty to assess the hypothesis of this study. A standard size hip implant with the cup radius 14 mm and the clearance size 30 μm is chosen, [24, 30]. The femoral head and the acetabular cup are assumed rigid. The lubricant is considered synovial fluid with a viscosity of 0.5 Pas to facilitate the numerical convergence. Three-dimensional physiological forces, Fig. 5, and angular motions obtained in vivo by Bergmann et al. are used, [25]. Moreover, the cup surface is discretized into several elements and the accuracy and convergence study are performed to evaluate the mesh density in order to solve the fluid equation using a finite difference

scheme. Consequently, a mesh grid of 250×250 elements on the cup surface is constructed. The computational method is stable and solutions to the equations always achieve. In the next section, the acquired values for velocity terms are compared to those from Goenka and Booker formulation. Moreover, the effect of modified velocities on fluid pressure and film thickness is investigated. The initial location of the femoral head for both solutions is (1.4, -5.57, 29.32) μm and its initial velocity is (-0.0052, 0.0018, 00.0006) m/s. Both models with the same initial conditions are simulated over four walking cycles to reach stable results. The outcomes acquired for the fourth walking cycle are used to evaluate the hypothesis of the present study.
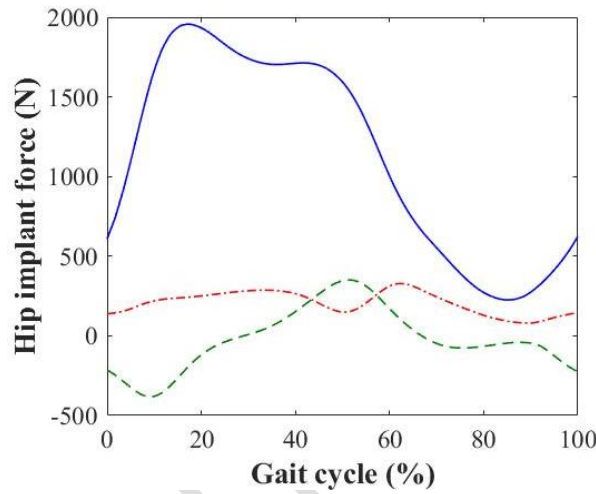

Fig. 5. Physiological adopted forces with ⸺ f_z (superior-inferior (SI)); ----- f_y (anterior-posterior (AP)); -·-·- f_x (medial-lateral (ML)) for the gait cycle.

In order to validate the model, the contribution of the modified velocity terms is ignored and a simplified problem introduced in [9] is considered with Goenka and Booker terms. In this problem, a hip implant subjected to just one angular velocity component and the vertical load component was considered. This problem is equivalent to the one of a sphere rolling on a plane that was studied by Kapitza [32]. In this early classical analysis, it was assumed that pressure was developed by hydrodynamic action only in the convergent film. The analytical solution by Kapitza can be rearranged to define a non-dimensional hydrodynamic parameter, D given in Table 1. The same set-up as presented in [9] was arranged and acquired results were compared to those reported by Jin and Dowson [9]. As it can be seen in Table 1, the minimum fluid-film thicknesses for different non-dimensional hydrodynamic parameter, D, comply with those from [9, 32].

Table 1. A comparison of the developed method with previous studies for the problem presented in [9].

	h_{min}/c			
$^{*}D = \dfrac{\left(\frac{R_c}{c}\right)^2 \omega^Z \mu R_c^2}{W^Y}$	Kapitza [32]	Goenka and Booker [7]	Jin and Dowson [9]	Present study
0.0083	0.001	——	0.0021	0.0021
0.01	0.0054	——	——	0.056
0.0198	0.0070	——	0.0072	0.0073
0.0375	0.0213	0.010	0.0156	0.0143

$^{*}W^Y = f_z \sin\beta + f_x \cos\beta$ and $\omega^Z = -\omega_x \sin\beta$ $(\beta = \frac{\pi}{4})$

3. Results and discussion

The velocity terms are calculated based on Eqs. (4) and (5), Goenka and Booker [7], as well as Eq. (6), the current study. Figs. 6a and 6b represent U_{Θ}-velocity profiles on the surface of the femoral head acquired with the modified velocity terms and the old velocities, respectively. It can be seen that U_{Θ}, Fig. 6a, varies with not only φ, but also Θ while that obtained using Goenka and Booker velocities is just a function of φ. Maximum velocities acquired for such velocity components corresponding to modified and old velocity terms are 0.0053 and 0.0012 m/s, respectively. In addition to maximum values, minimum speeds are -0.0099 and -0.0060 m/s corresponding to Fig. 6a and 6b, respectively. The same scenario takes place for the case of U_{φ}-velocity component as velocity profiles, shown in Fig. 6c and 6d, reveal different trends. The corresponding maximum speeds are 0.0091 and 0.0060 while the minimum values are -0.0124 and -0.0084 m/s, respectively. Therefore, it can be concluded that velocities used in the Reynolds equation should include both rotational and translational motions and neglecting translational term is not acceptable in calculating such velocities.
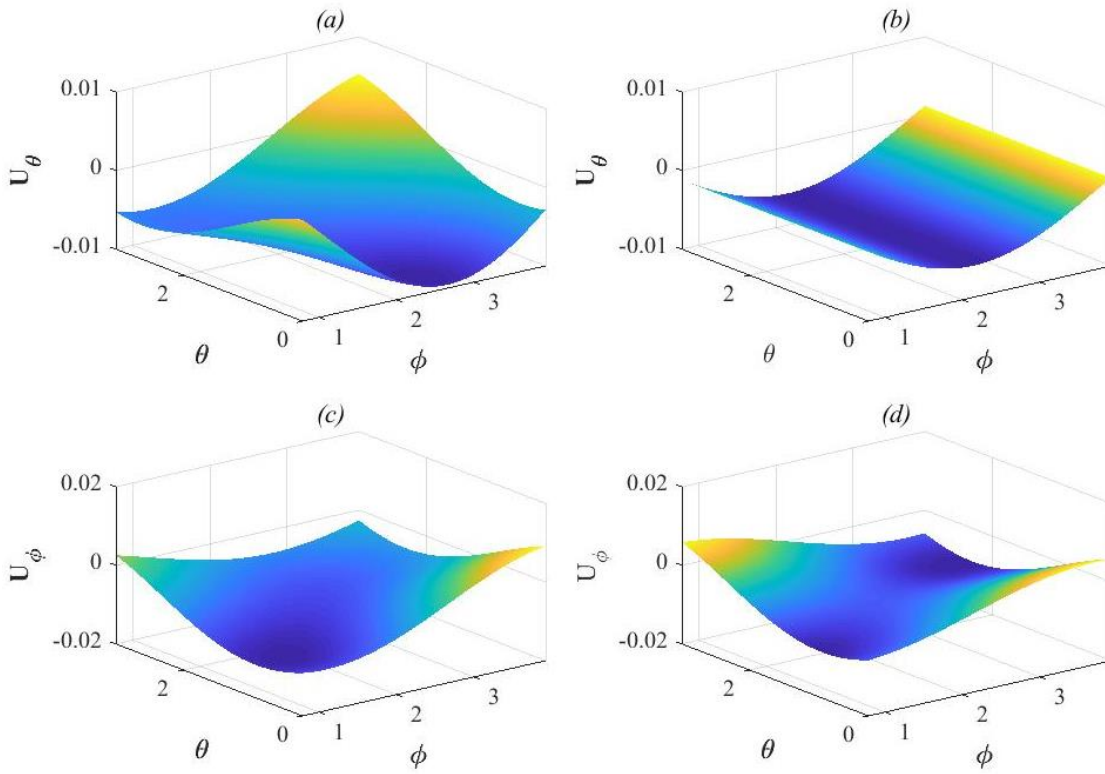
Fig. 6. Surface plots of velocity terms over the fluid domain: U_θ (*m/s*) obtained by (*a*) modified velocity terms and (*b*) old velocity terms; U_φ (*m/s*) acquired by (*c*) modified velocity terms and (*d*) old velocity terms. Θ and φ are given in degrees.

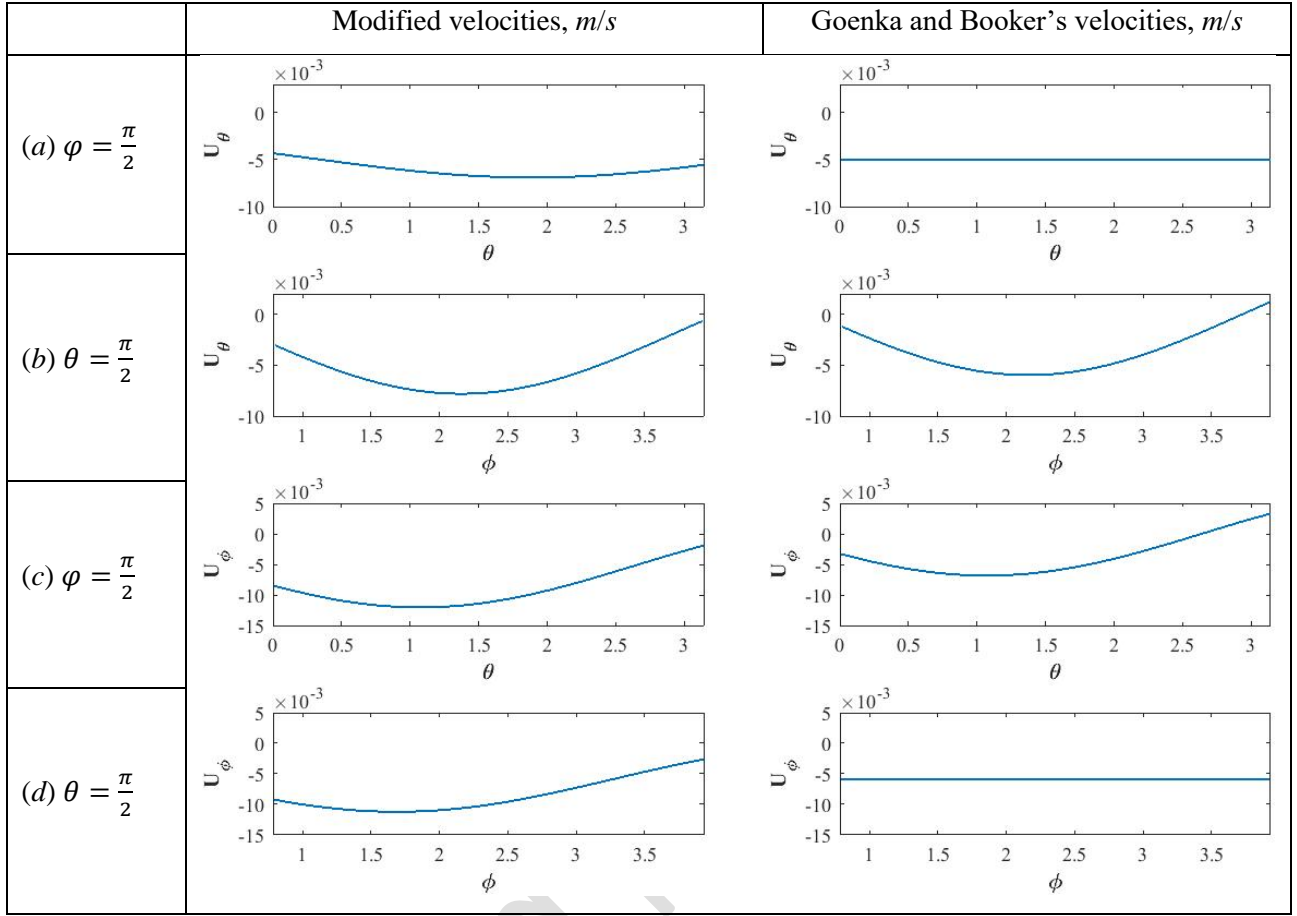|	Modified velocities, *m/s*	Goenka and Booker's velocities, *m/s*
(a) $\varphi = \frac{\pi}{2}$		
(b) $\theta = \frac{\pi}{2}$		
(c) $\varphi = \frac{\pi}{2}$		
(d) $\theta = \frac{\pi}{2}$		

Fig. 7. A comparison of velocity terms at two cross sections of the cup, namely $\varphi = \frac{\pi}{2}$ and $\Theta = \frac{\pi}{2}$. Velocities are determined with angular velocities: $\omega_x = 0.3564$, $\omega_y = 0.2348$ and $\omega_z = -0.4262$ (rad/*s*).

Moreover, velocities are obtained and plotted in Fig. 7 along two cross sections of the acetabular cup, $\varphi = 90°$ and $\Theta = 90°$. In the right-side plot of Fig. 7a, it can be seen that U_Θ gains a constant value acquired from Eq. (4) while that from Eq. (6) shown in the plot on the left side provides a varying curve for velocity along the cross section defined by $\varphi = 90°$. U_Θ and U_φ velocities in these two cross sections, observable in Fig. 7, demonstrate that the translational motion of the femoral head affects the tangential velocities contributing to the fluid lubrication. In Fig. 7d, U_φ obtained by the Goenka and Booker velocity terms is a constant value due to $\Theta = 90°$, Eq. (5), but the velocity obtained from the modified velocities depicts a variation from -6.9 to -4.4 mm/s. It is worth noting that these results are calculated at the first time step of the simulation, i.e. $t = 0$ *s*, where the corresponding physiological angular velocities are as reported in the caption of Fig. 7. Moreover, velocity profiles illustrated in Figs. 6 and 7 are not initial conditions of the coupled system, but are exactly what the present article aims to address, which is the importance of considering the translational motion. The initial conditions applied to the equations of the coupled system are those reported in the section

2.5., i.e. the initial position and velocity of the femoral head in the original coordinate system whose origin locates at the cup center.
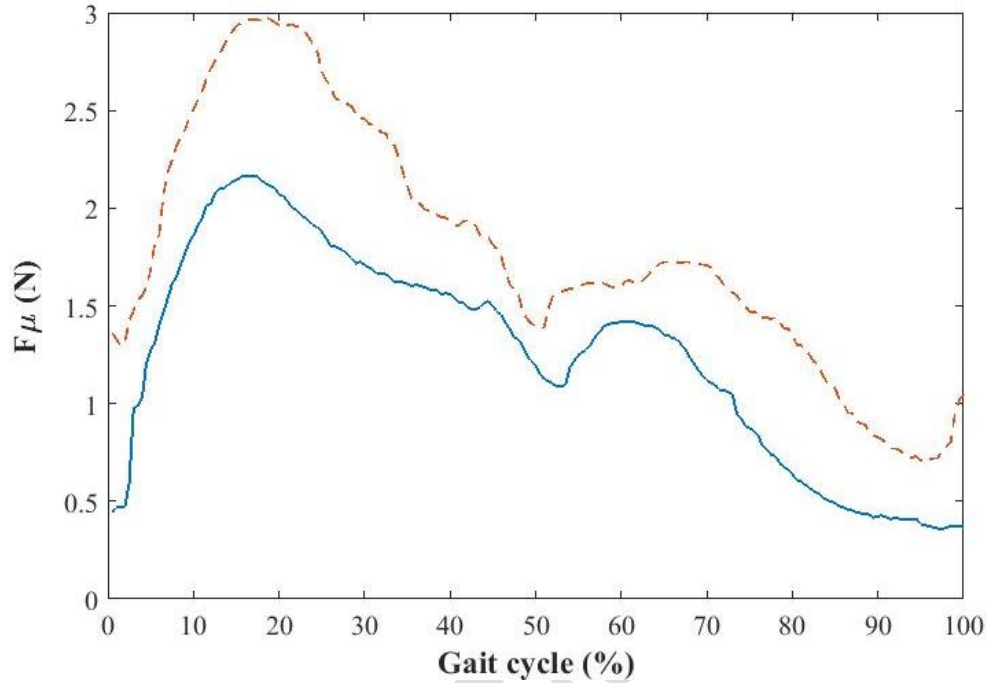

Fig. 8. Friction force, due to fluid shear stresses, applied to the femoral head with Goenka and Booker's velocity terms (solid line) and modified velocity terms (dashed line).

Friction force calculated from friction-force components obtained from Eq. (19) are reported in Fig. 8. According to the variation seen in velocities, Figs. 6 and 7, it can be deduced that velocity terms can affect friction forces since the first term on the right-hand side of Eqs. (20-22) are directly proportional to the velocity. In addition, one can argue that pressure and film thickness can be influenced by velocities used in Reynold equation. Fig. 8 represents the trend of friction forces over a full walking cycle. The velocities obtained by Eq. (6) are greater than those from Eqs. (4) and (5), thereby reasoning that friction forces can be greater than those predicted by Goenka and Booker [7]. Both trends show an overall increase of friction force until 18% of the gait due to increasing physiological angular velocities before a decrease is observed up to the half of the gait. Thereafter, friction force undergoes an increase before decaying again. The friction force obtained from the modified velocity terms rises at the end of the walking cycle while that of Goenka and Booker's keeps decreasing. It is worth noting that friction-force values are small compared to those resulted from pressure itself. However, these loads contribute to friction-induced vibration and help to satisfy no-slip boundary conditions. Generally, the friction increases when film thickness decreases and lubrication regime goes from full film to either mixed lubrication or boundary lubrication. Stribeck [33] suggested a

model known as the Stribeck model, which can convey the friction behavior of an articulation in different lubrication regimes.
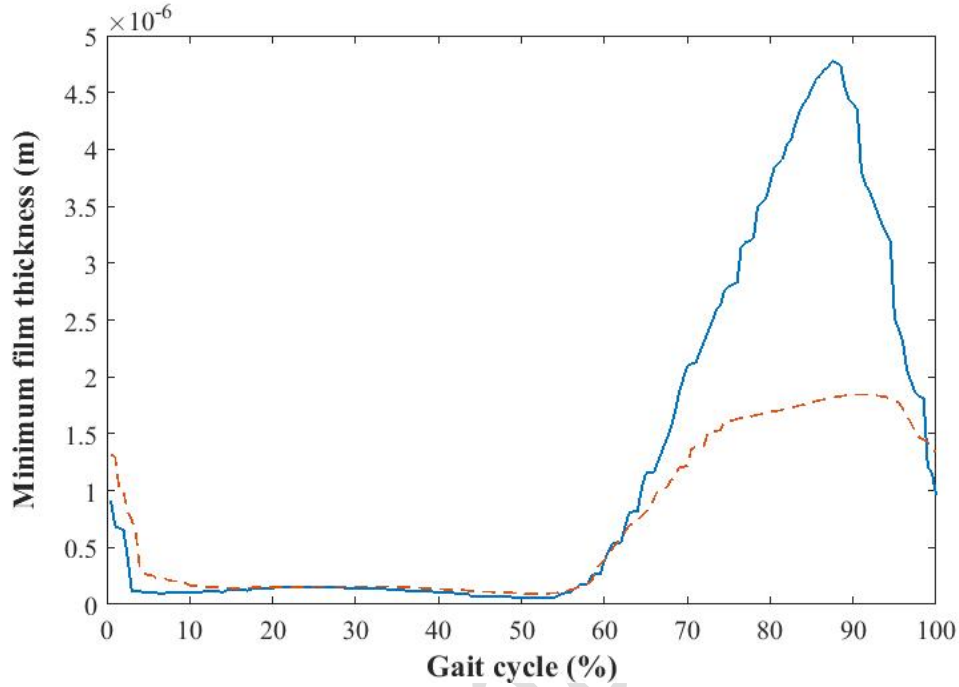

Fig. 9. Minimum fluid-film thickness obtained with Goenka and Booker's velocity terms (solid line) and modified velocity terms (dashed line).

In addition, the fluid-film thickness, h_{min}, is a crucial parameter in studying fluid-film lubrication in hip implants, from which the regime of lubrication can be determined. Regarding the Lambda number, if h_{min} is three times as big as the equivalent roughness of bearing surfaces, a full-film lubrication is generated, thereby keeping bearing components separated from each other [3, 34]. However, if the magnitude of minimum-film thickness falls below the roughness value it leads to a boundary lubrication where dry contact occurs and the highest friction coefficient and wear coefficient are observed, resulting in higher wear rates of articulating surfaces. The mixed lubrication is another possible scenario where surface asperities of two components contact each other. Therefore, the effect of velocity terms on minimum fluid-film thickness is considered and presented in Fig. 9. Both models show a similar trend, although the film thickness obtained from the model with old velocity terms are considerably greater than that with the modified velocities during the swing phase. The translation causes the tangential velocity to decrease during the swing phase, which can be considered a reason for such a difference observed between results. An opposite scenario can be seen during the stance phase where the results associated with the modified velocity terms are greater than those acquired from that with the Goenka and Booker velocities. Fluid-film thickness obtained here are less during the stance phase, but greater during the swing phase than those reported by Jin and Dowson [9] because the

squeeze-film action is neglected in the present study as well as using different loadings and motion, and geometrical properties, although the viscosity taken by the present study is bigger than that in [9].

The elastic deformation of hip components are neglected in the present study as hip components are assumed to be made of hard materials, although it is not a physically accepted assumption (see the paragraph after Fig. 10). If one considers hip components made of alumina with Young's modulus of 380 GPa, the alumina average roughness is 0.001 μm [3]. Therefore, the composite roughness of the couple of bearings is 0.0014 μm. The minimum film thickness for a full gait, illustrated in Fig. 9, is 0.06 μm and the corresponding lambda ratio (λ) computed is more than 40, which means the type of lubrication regime is fluid-film lubrication. Hence, there is no need to take asperity contacts into account. However, if hip components are made of CoCrMo with Young's modulus of 230 GPa, the average roughness is 0.01-0.05 μm and the fluid lubrication as considered in the present study can undergo all three lubrication regimes, namely boundary lubrication, mixed lubrication and fluid-film lubrication, in such a roughness range somehow. Asperity contacts should, therefore, be taken into account. The present study, however, aims to modify velocity terms used in Reynolds equation rather than to investigate roughness effects on fluid lubrication and hip articulation.
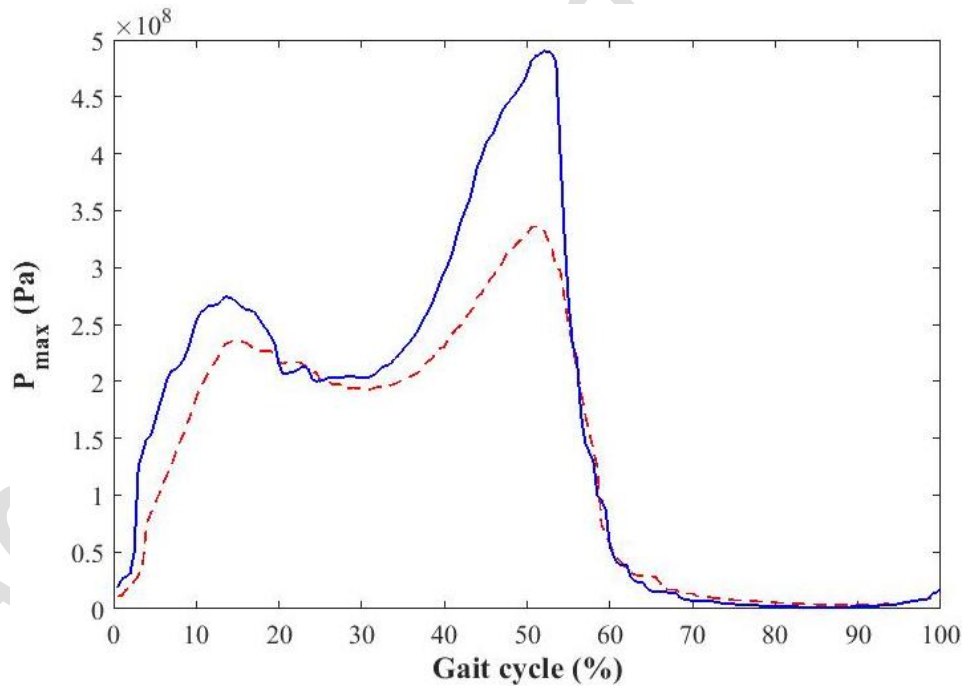

Fig. 10. Maximum fluid pressure obtained with Goenka and Booker's velocity terms (solid line) and modified velocity terms (dashed line).

The influence of velocity terms is also considered on the maximum fluid pressure and corresponding outcomes are presented in Fig. 9. The general trend shows that the maximum fluid pressure obtained using

the modified velocities in Reynolds equation is less than that from Goenka and Booker during the stance phase while an opposite scenario is seen during the swing phase. The maximum differences between fluid pressures of these two models take place close to two loading peaks. At the second peak, the maximum pressure obtained from the old velocity terms shows a 50% increase compared to that of the modified velocities. The maximum fluid pressure observed in Fig. 10 is just less than 490 MPa while the minimum pressure is 1.5 MPa. Regarding the piezoviscosity phenomenon, the viscosity of many lubricants increases with pressure [35]. When surfaces in contact are sufficiently hard, the lubricant pressure may increase significantly, as it happens in the problem at hand. It is known that the lubricant loses its liquid character and becomes semi-solid under some constraints, e.g. high pressure. It has been reported by Jin and Dowson, [9], that it is not clear how synovial fluid may behave under excessive contact pressures. However, the elastic deformation of hip components helps the maximum pressure go below 60 MPa for metal-on-metal hip implants and 15 MPa for polyethylene hip prostheses, [12-13]. Thus, the elasticity of bearing surfaces constituting the hip articulation should be taken into account. It is worth mentioning that the present paper does not take elastic deformation of hip components into account, which will be considered in future studies using the modified velocity terms.

Moreover, the governing equations of both multibody dynamics and computational fluid dynamics are strongly nonlinear. Such nonlinearity leads to solutions depending upon initial conditions assigned during the numerical set-up. In fact, the initial location of the femoral head with respect to the cup in vivo is not known and varies according to for example switching from one activity to another. Thus, both maximum fluid pressure and minimum film thickness can evolve during few first walking cycles before a stable solution is achieved. In the first walking cycle, a high maximum fluid pressure occurs due to the non-stable situation. Thereafter, the pressure decreases smoothly until it becomes invariant by walking cycle. It is worth mentioning that the problem does not have a unique solution under the same loadings and properties until a stable state is achieved after a sufficient number of walking cycles. The effect of number of walking cycles on hydrodynamic and elastohydrodynamic lubrication of hip prostheses as well as the stable solution will be reported and discussed in another paper.

4. Conclusion

The present study hypothesized that using modified velocity terms, accounting for both the rotational and translational motions of the femoral head, can affect velocity terms, resultant fluid pressure, minimum fluid-film thickness and frictional force. The hypothesis was tested by developing a dynamic model of hip arthroplasty based on the multibody dynamics methodology subjected to a normal walking condition. The fluid flow was formulated using Reynolds equation and the finite difference method was employed to discretize the fluid equation. The Gauss-Seidel relaxation method and multi-grid approach were implemented

to solve Reynolds equation. Fluid-structure interaction was considered using a partitioned method. The hypothesis of the current study was confirmed reporting considerable differences between modified velocity terms and those by Goenka and Booker. Moreover, it was shown that frictional force increased using the modified velocities compared to those terms excluding the translation of the femoral head. Although a decreasein maximum fluid pressure was observed during the stance phase, fluid pressure rises during the swing phase with respect to the case in which the old speed terms were employed. An opposite trend was also observed for the minimum film thickness. It can, therefore, be concluded that neglecting the translation of the femoral head when computing the velocity of any point on the head surface is not acceptable and that future studies should consider using the modified velocities presented in the present study.

Acknowledgements

References

[1] Stachowiak, G.W., Batchelor, A.W., Engineering tribology. Elsevier, 1993.

[2] Attia, H.M., Bouziz, S., Maatar, M., Fakhfakh, T., Haddar, M., Hydrodynamic and elastohydrodynamic studies of a cylindrical journal bearing. J Hydrodyn 2010;22(2):155–63.

[3] Askari, E., Flores, P., Dabirrahmani, D., Appleyard, R. A review of squeaking in ceramic total hip prostheses. Tribology International 2016;93:239-256

[4] Reynolds, O. 1886. On the Theory of Lubrication and Its Application to Mr. Beauchamp Tower's Experiments, Including an Experimental Determination of the Viscosity of Olive Oil. Philosophical Transactions of the Royal Society of London.

[5] Pinkus, O. and Sternlicht, S.A., Theory of Hydrodynamic Lubrication, McGraw-Hill, New York, 1961.

[6] Hamrock, B.J., Fundamentals of Fluid Film Lubrication, McGraw-Hill, New York, 1994.

[7] Goenka, P.K., Booker, J.F., Spherical bearings: static and dynamics analysis via the finite element method. ASME J Lubr Technol 1980;102(7):308-319.

[8] Ai, X., Cheng, H.S., Hydrodynamic lubrication analysis of metallic hip joint. Tribol Trans 1996;39(1):103–11.

[9] Jin, Z.M., Dowson, D., A full numerical analysis of hydrodynamic lubrication in artificial hip joint replacements constructed from hard materials. Proc IMECHE, J Mech Eng 1999;213(4):355–70.

[10] Hamrock, B.J., Dowson, D., Elastohydrodynamic lubrication of elliptical contacts for materials of low elastic modulus I – fully flooded conjunction. J Tribol 1978;100(2).

[11] Jagatia, M., Jin, Z.M., Elastohydrodynamic lubrication analysis of metal-on-metal hip prostheses under steady state entraining motion. Proc IMECHE, J Eng Med 2001;215(H6):531–41.

[12] Jagatia, M., Jalali-Vahid, D. and Jin, Z. M. Elastohydrodynamic lubrication analysis of UHMWPE hip joint replacements under squeeze-film motion. Proc. Instn Mech. Engrs, Part H: J. Engineering in Medicine, 2001;215(H2):141-152.

[13] Gao, L.M., Wang, F.C., Yang, P.R., Jin, Z.M., Effect of 3D physiological loading and motion on elastohydrodynamic lubrication of metal-on-metal total hip replacements. Med Eng Phys 2009;31:720–729.

[14] Gao, L., Fisher, J., Jin, Z., Effect of walking patterns on the elastohydrodynamic lubrication of metal-on-metal total hip replacements. Proc Inst Mech Eng Part J J Eng Trib 2011;225:515–525.

[15] Sonntag, R., Reinders, J., Rieger, J.S., Heitzmann, D.W.W., Kretzer, J.P., Hard-on-hard lubrication in the artificial hip under dynamic loading conditions. PLoS One 2013;8:e71622.

[16] Jin, Z.M., Theoretical studies of elastohydrodynamic lubrication of artificial hip joints. Proc Inst Mech Eng Part J J Eng Trib 2006;220:719-727.

[17] Jalali-Vahid, D., Jin, Z.M., Transient elastohydrodynamic lubrication analysis of UHMWPE hip joint replacements. Proc IMECHE, J Mech Eng 2002;216 (C4): 409-420.

[18] Liu, F., Jin, Z.M., Grigoris, P., Hirt, F., Rieker, C., Steady state elastohydrodynamic lubrication analysis of a metal-on-metal hip implant employing a metallic cup with an ultra-high molecular weight polyethylene backing. Proc. Instn Mech. Engrs, Part H: J. Engineering in Medicine 2004;218:261-270.

[19] Wang, F.C., Jin, Z.M., Prediction of elastic deformation of acetabular cup and femoral head for lubrication analysis of artificial hip joints. Proc Inst Mech Eng Part J J Eng Trib 2004;218:201-209.

[20] Gao, L., Dowson, D., Hewson, R.W., A numerical study of non-Newtonian transient elastohydrodynamic lubrication of metal-on-metal hip prostheses. Tribol Int 2016;93:486-494.

[21] Szeri, A.Z. Fluid film lubrication: theory and design. Cambridge University Press, 1998.

[22] Flores, P., Lankarani, H.M., Spatial rigid-multi-body systems with lubricated spherical clearance joints: modeling and simulation. Nonlinear Dyn. 2010;60:99-114.

[23] Askari, E., Flores, P., Dabirrahmani, D., Appleyard, R., A computational analysis of squeaking hip prostheses. J Comput Nonlinear Dyn 2015;024502:1-7.

[24] Askari, E., Flores, P., Dabirrahmani, D., Appleyard, R., Nonlinear vibration and dynamics of ceramic on ceramic artificial hip joints: a spatial multibody modelling. Nonlinear Dyn 2014;76(2):1365-1377.

[25] Bergmann, G., Deuretzbacher, G., Heller, M., Graichen, F., Rohlmann, A., Strauss, J., et al., Hip contact forces and gait patterns from routine activities. J. Biomech. 2001;34(7):859-871.

[26] Askari, E., Flores, P., Dabirrahmani, D., Appleyard, R., Study of the friction-induced vibration and contact mechanics of artificial hip joints. Tribol Int 2014;70:1-10.

[27] Flores, P. Ambrósio, J., Claro, J.P., Dynamic analysis for planar multibody mechanical systems with lubricated joints, Multibody Syst. Dyn. 2004;12:47-74.

[28] Askari, E., Flores, P., Dabirrahmani, D., Appleyard, R., Dynamic modeling and analysis of wear in spatial hard-on-hard couple hip replacements using multibody systems methodologies. Nonlinear Dyn 2015;82:1039-1058.

[29] Gao, L.M., Wang, F.C., Yang, P.R., Jin, Z.M., Effect of 3D physiological loading and motion on elastohydrodynamic lubrication of metal-on-metal total hip replacements. Med Eng Phys. 2009;31:720-729.

[30] Brandt, A., Multi-Level Adaptive Solutions to Boundary-Value Problems. Math. of Comp. 1977;31(138):333-390.

[31] Venner, C.H., Multilevel solution of the EHL line and point contact problems. PhD thesis, University of Twente, Enschede (N.L.), 1991.

[32] Malvandi, A., Ghasemi, A., Nikbakhti, R., Ghasemi A., Hedayati, F., Modeling and parallel computation of the non-linear interaction of rigid bodies with incompressible multi-phase flow. COMPUT MATH APPL 2016;72:1055-1065.

[33] Sanders, J., Dolbow, J. E., Mucha, P. J. and Laursen, T. A., A new method for simulating rigid body motion in incompressible two-phase flow, INT J NUMER METH FL 2011;67:713-732.

[34] Stribeck, R., Die wesentlischen Eigenschaften der Gleit- und Rollenlager - The key qualities of sliding and roller bearings. Zeitschrift des Vereines deutscher Ingenieure 1902;46(37):1341-1348 (pt I) & 46(38):1432-1438 (pt II) & 46(39) 1463-1470 (pt III).

[35] Mattei, L., Di Puccio, F., Piccigallo, B., Ciulli, E., Lubrication and wear modelling of artificial hip joints: a review. Tribol Int 2011;44(5):532-549.

[36] Stachowiak, G.W., Batchelor, A.W., Engineering tribology. Elsevier, 1993.

[37] Kapitza, P.L. Hydrodynamic theory of lubrication during rolling. Zh. Tekh. Fiz. 1955;25(4):747-762.